Device Classification Performance Modeling Using UWB Stimulated RF-DNA Fingerprinting

M. W. Lukacs,[1] P.J. Collins,[1] and M. A. Temple[1]

Corresponding author: M. W. Lukacs, Department of Elec. and Comp. Eng, Air Force Institute of Technology, Wright Patterson AFB, OH 45433, USA. (mathew.lukacs@afit.edu)

[1]Department of Elec. and Comp. Eng,
Air Force Institute of Technology, Wright
Patterson AFB, OH 45433, USA.

Abstract. Quality control is critical for all industrial processes, but often times defect detection is labor intensive. A novel approach to industrial defect detection is proposed using a Digital Noise Radar (DNR), coupled with Radio Frequency Distinct Native Attribute (RF-DNA) fingerprinting processing algorithms to non-destructively interrogate microwave devices. The DNR is uniquely suitable since it uses an Ultra Wideband noise waveform as an active interrogation method that will not cause damage to sensitive microwave components. Additionally, it has been demonstrated that multiple DNRs can operate simultaneously in close proximity, allowing for significant parallelization of defect detection systems resulting in increased process throughput. Using this method, 100% sampling for quality control may be attainable in many cases.

The ability to classify defective units from properly functioning units was demonstrated in *Lukacs et al.* with potential applications including assembly line inspection of automotive collision avoidance systems, wireless or cellular antenna defect detection during manufacture, and phased array element defect detection prior to RF system assembly. However, prior research into active interrogation has been strictly empirical. This paper will develop an analytical model and simulation for interrogating a passively terminated antenna with an overall objective of improving classification performance through optimization of the interrogation signal bandwidth.

1. Introduction

RF-DNA fingerprint processing is a method to extract features received from a Radio Frequency (RF) signal [*Klein et al.*, 2009]. The concept is based on the fact that every device emits signals that have unique characteristics that can be used to distinguish that device from other, similar devices [*Zeqolari*, 2014]. The term "fingerprinting" is used because the concept is similar to human fingerprinting, where a person's fingerprints can be used to distinguish them from another person [*Klein et al.*, 2009]. RF-DNA fingerprinting has been in development at Air Force Institute of Technology (AFIT) since 2006 successfully demonstrating feature extraction from RF emissions received from various devices including IEEE 802.11 WiFi, IEEE 80211.15 BlueTooth, IEEE 802.16 WiMAX, Global Systems for Mobile Communications (GSM) cell phones, and Radio Frequency Identification (RFID) emitters [*Reising*, 2012]. To date, all of these methods have been performed in a passive manner, whereby the signals analyzed by the RF-DNA fingerprint processing algorithms were already generated by the device under normal operation. This works well for devices that normally broadcast some RF emission that can be exploited. However, a whole class of devices exist that do not normally emit RF radiation, such as properly shielded RF amplifiers, mixers, oscillators and filters that make up a typical receiver front-end. The potential exists for these devices to be classified using an "active" interrogation method, such as a radar transmission. The RF energy of the radar will be reflected by the device in a manner that can be exploited by RF-DNA fingerprint analysis [*Lukacs et al.*].

Instead of a traditional narrow-band radar signal for interrogation, this paper investigates the use of an Ultra Wideband (UWB) noise signal from a DNR as the interrogation waveform, specifically the effect of bandwidth on classification performance. An UWB signal has a much larger frequency content than a traditional narrow band signal. As such an UWB signal may provide increased classification performance as an interrogation signal because of the larger instantaneous bandwidth [*Zeqolari*, 2014]. For instance, the UWB signal may excite resonant structures in a specific target (such as a Log Periodic Antenna (LPA)), resulting in larger signal energy returns within specific frequency bands which can be used for classification of the radar target [*Ludwig*, 2012]. The bandwidth requirements of an UWB Digital Noise Radar drive the design requirements of the system. Ideally, a noise source with infinite bandwidth with a flat spectral response is available for classification, but this is unrealizable; all signals are band limited and it is important to be able to thoroughly characterize the impact of signal bandwidth on classification performance.

2. RF-DNA Fingerprintin

Statistical RF-DNA fingerprints consist of features that are generated by the statistical properties of fixed regions within the received signal [*Klein et al.*, 2009]. The RF-DNA fingerprint process extracts features using three instantaneous responses: the Instantaneous Amplitude (IA) response, $a(n)$, the Instantaneous Phase (IP) response, $\phi(n)$, and the Instantaneous Frequency (IF) response, $f(n)$. The standard deviation (σ), variance (σ^2), skewness (γ) and kurtosis (κ) are generated for each response. These statistics are

calculated using the following equations:

$$\sigma^2 = \frac{1}{N_x}\sum_{n=1}^{N_x}(\bar{x}_c(n) - \mu)^2, \tag{1}$$

$$\gamma = \frac{1}{N_x}\sigma^3\sum_{n=1}^{N_x}(\bar{x}_c(n) - \mu)^3, \tag{2}$$

$$\kappa = \frac{1}{N_x}\sigma^4\sum_{n=1}^{N_x}(\bar{x}_c(n) - \mu)^4 \tag{3}$$

where $\bar{x}_c(n)$ is the normalized data sequence with N_x samples, and each of the above statistics is calculated over an equal, contiguous, sub-region of $\bar{x}_c$. These sub-regions are determined empirically and are application specific. For the UWB experiment in section 5 five equal sub-regions were used. In each of the five sub-regions, standard deviation and the three statistics calculated in (1), (2) and (3) are concatenated to form "distinct native attribute marker" to the sub-regional RF-DNA vector, i, according to [*Klein et al.*, 2009]:

$$F_{R_i} = \left[\sigma_{R_i}\ \sigma^2_{R_i}\ \gamma_{R_i}\ \kappa_{R_i}\right]_{1x4}.$$

After which, each distinctive native attribute marker vector is concatenated to form a "composite characteristic vector" according to [*Klein et al.*, 2009]:

$$F^C = \left[F_{R_1} \vdots F_{R_2} \vdots \cdots F_{R_{N_R+1}}\right]_{1x4(N_R+1)},$$

in which C denotes the analyzed response (IA, IP or IF), and N_R is the total number of sub-regions. Each of the composite characteristic vectors are finally concatenated into one statistical fingerprint (of 60 elements for 5 sub-regions) according to [*Klein et al.*, 2009]:

$$F = \left[F^a \vdots F^\phi \vdots F^f\right]. \tag{4}$$

2.1. Multiple Discriminant Analysis / Maximum Likelihood

Multiple Discriminant Analysis (MDA) is not, by itself, a classifier [*Duda et al.*]. It is an algorithm to achieve dimensionality reduction of a multi-dimensional dataset such that

a more traditional classifier can be applied, e.g., a Maximum Likelihood (ML) classifier. Multiple Discriminant Analysis / Maximum Likelihood (MDA/ML) aims to project from a d-dimensional space to a $(c-1)$ dimensional space, where c is the number of distinct classes (it is assumed the $d \geq c$, or some space of dimension greater than c). Figure 1 is a example of MDA/ML applied to a 3-dimensional dataset. In the figure, the MDA/ML algorithm is used to project the 3-dimensional space into two, 2-dimensional sub-spaces. The 2-dimensional sub-spaces are defined by their norm vectors, W_1 and W_2 respectively. The algorithm attempts to find the optimal sub-space for classification, by finding one with the greatest separation of the projected distributions of the classes. For instance, discrimination along the W_1 sub-space would be considerably easier than across the W_2 sub-space that still has overlapping projections. For higher class problems, it becomes difficult to visualize in a 3-dimensional space.

3. Proposed Transmission Line Model

The "target" for the research conducted is a passively terminated UWB antenna. Previous experimentation using both LPA and Ultra High Frequency (UHF) antennas as the transmit and receive antennas on a UWB Digital Noise Radar has been conducted at AFIT for several years [*Priestly*, 2011; *Hardin*, 2013; *Zeqolari*, 2014; *Schmitt*, 2009; *Ludwig*, 2012; *Wilson and Collins*, 2013]. For this model, an electromagnetic plane wave signal, generated from an UWB digital noise radar, propagating in free-space, is incident on the bore sight direction of a passively terminated antenna. The reflected signal received at the noise radar is then processed using a digital correlator which can be used for various purposes to include ranging information and RF-DNA based classification.

3.1. Scatter

The use of an antennas as a target model effectively categorizes the system response as an electromagnetic scatter problem. Scattering is the effect of removing energy from a propagating electromagnetic wave, and re-radiating it with potential changes in direction, phase or wavelength [*Lynchi*, 2004]. For electromagnetic scattering, some of the energy incident on the antenna is absorbed and some is re-radiated towards the receiving antenna. The three major types of scatter from the antenna are: antenna-mode scattering, σ_s, antenna-structural scattering, σ_a and RCS grating [*Lynchi*, 2004]. The structural mode scattering is from the physical shape of the antenna, material composition, geometry as well as the orientation. The antenna-mode scattering is due to the internal reflections inside the antenna, including reflections off of the termination for the proposed passively terminated antenna model. Grating lobes are areas of increased radiation in non-bore sight directions on linear arrays, and have no real relevance for the proposed system model. Additionally, it is assumed that the incident wave polarization is matched to the "target" antenna, since some antennas (such as dipoles) have little to no backscatter for unmatched polarizations [*Lynchi*, 2004].

For the structural scattering mode, which is based on various structural characteristics of the antenna, the Radar Cross Section (RCS) will remain fixed at a given incident angle. However, for the antenna mode scattering, the RCS is based on the termination load and the antenna impedance. For the purposes of this research, it is assumed that the antenna impedance is designed to be 50Ω across the bandwidth of the UWB antenna.

3.2. Filter Model

The spatial aspect of the filter model concept concerns antenna directivity. For the research conducted within this paper, the incident electrical field is modeled as a plane wave incident on the bore sight of the antenna, or the axis with maximum gain. A key assumption is that the direction of the bore sight does not change with frequency. Therefore, both the transmit mode and receive mode of the antenna can be modeled with an impulse response $h(t, \theta, \psi)$ in the time domain and corresponding transfer function $H(\omega, \theta, \psi)$ in the frequency domain. The impulse response and transfer function is reciprocal for both transmit and receive ($H_{Tx}(\omega, \theta, \psi) = H_{Rx}(\omega, \theta, \psi)$), with the exception of the signal vector direction. Since we are only concerned with the boresight direction of the same antenna, separate transmit and receive transfer functions are unnecessary [*Wiesbeck et al.*, 2009].

The transfer function of the antenna only models the the energy propagating through the antenna. The received transfer function, H_{Rx} is defined as the relationship between the incident electromagnetic field, $E_{Rx}(f, r)$ to the voltage output at the antenna terminals, $U_{Rx}(f)$, and likewise for the transmitted transfer function, H_{Tx} [*Wiesbeck et al.*, 2009]. These transfer functions do not take into account the structural-mode scatter or the antenna-mode scatter mentioned previously. However, for the proposed antenna-target, antenna-mode reflections off of the antenna loading will be captured by the cascaded receive and transmit transfer functions.

In order to investigate the effect of signal bandwidth on classification capability of the RF-DNA tools, the antenna can either be modeled as a low-pass filter or a band-pass filter. [*Ludwig*, 2012] showed that the bandwidth of the LPA antennas used in the AFIT DNR, and proposed as the target antenna, has an approximate bandwidth of 400 - 750 MHz, which can be modeled as a bandpass filter. The cross-correlation response is affected

by the center frequency of the interrogation signal, therefore the bandpass filter can be tuned not only to a different bandwidth, but also a different center frequency. Finally, to simulate the effect of a more ideal UWB signal with a much larger frequency content, a low pass filter can be employed. The resonant modes of a LPA will be difficult to model with a bandpass filter, but for the purposes of this research, the resonant effect is not really necessary and could serve only to complicate the model.

3.3. Time Dispersion

Modeling an antenna as a filter means that it has a magnitude and phase response, $H(f) = A(\omega)e^{j\theta(w)}$ [*Mohammadian et al.*, 2003]. Filters will distort the input signal, instilling both amplitude and phase distortions. These distortions comprise the group delay of the filter, which indicates how much time delay the filter imposes on the input signal at specific frequencies. This is a good measure of the time dispersion of the antenna. A linear filter will have an ideally constant group delay, meaning that all frequencies are time delayed by approximately the same amount resulting in little distortion of the output signal. An antenna, modeled as a filter, will have a similar effect. Some UWB antennas are fairly linear, such as Vivaldi antennas. However, other antennas, such as the LPA, have non-linear group delays (due to the frequency dependent phase-center of the LPA). A non-linear group delay is indicative of an ability for the antenna to store energy and causes resonances [*Wiesbeck et al.*, 2009]. These resonances will result in oscillations and "ringing" of the output time signal. When used for a communications link or similar purposes, the resonance is a hindrance to performance and antenna engineers frequently try to mitigate or linearize the antenna group delay. However, for classification purposes, the frequency dependent resonance adds to the character of the antenna and can result in

improved classification. The group delay is based on the phase difference between the input and output signals, which is directly affected by the antenna loading conditions, therefore the group delay will assist in classifying different termination conditions. Additionally, the bandwidth of the interrogation waveform and antenna frequency response will have a direct effect on group delay. A narrow-band interrogation pulse will experience a constant linear group delay whereas a wider bandwidth will experience the non-linear group delays, which will translate to a distorted signal that is useful for classification purposes.

4. Analytical Model Derivation

The relationship between the received voltage of an antenna, $u_{rx}(t, r, \theta, \psi)$ and the electrical field incident on the antenna boresight, $e_i(t, r, \theta, \psi)$, can be modeled in both the time domain and frequency domain as [*Papio-Toda et al.*, 2007]:

$$\frac{u_{rx}(t, r, \theta, \psi)}{\sqrt{Z_c}} = \mathbf{h}(t, \theta, \psi) * \frac{e_i(t, r, \theta, \psi)}{\sqrt{Z_0}} \tag{5}$$

$$\frac{U_{rx}(\omega, r, \theta, \psi)}{\sqrt{Z_c}} = \mathbf{H}(\omega, \theta, \psi)\frac{E_i(\omega, r, \theta, \psi)}{\sqrt{Z_o}} \tag{6}$$

where Z_c and Z_0 are the antenna characteristic impedance and free space impedance respectively. Generally, $\mathbf{h}(t, \theta, \psi)$ and $\mathbf{H}(\omega, \theta, \psi)$ are dependent on the direction of arrival of the incident wave in (θ, ψ) space, but since we are only concerned with the bore sight arrival, the model for $\mathbf{h}(t, \theta, \psi)$ and $\mathbf{H}(\omega, \theta, \psi)$ can be limited for model simplicity.

Antenna transmission is similar to reception, but with a significant difference. The transmit impulse response is actually the first-order time derivative of the receive impulse response [*Papio-Toda et al.*, 2007]. This is a consequence of the well known Lorentz Reciprocity constraint applied to Maxwell's curl equations [*Di Benedetto et al.*, 2006]. Therefore, the time domain and frequency domain transmission antenna response can be

modeled as [*Papio-Toda et al.*, 2007]:

$$\frac{e_i(t,r,\theta,\psi)}{\sqrt{Z_0}} = \frac{1}{r}\delta\Big(t-\frac{r}{c}\Big) * \Big[\frac{1}{2\pi c}\frac{\partial}{\partial t}\mathbf{h}(t,\theta,\psi)\Big] * \frac{u_{tx}(t)}{\sqrt{Z_c}} \tag{7}$$

$$\frac{E_i(\omega,r,\theta,\psi)}{\sqrt{Z_0}} = \frac{e^{-j\omega r/c}}{r}\Big[\frac{jw}{2\pi c}\mathbf{H}(\omega,\theta,\psi)\Big]\frac{U_{tx}(\omega)}{\sqrt{Z_c}} \tag{8}$$

where e_i is the electric field intensity at distance r from the antenna and u_{tx} is the voltage incident on the antenna input terminals. Eq. 7 has a convolution with the Dirac-delta function, which is necessary to account for slowing due to the speed of light, c. As indicated above, the impulse response for transmission is related to the time-derivative of the impulse response for the receive case. This means that the antenna is going to radiate the time-derivative of the input voltage, which in the proposed circuit model, is the reflected voltage off of the antenna load. The gain of the antenna, $G(f,\theta,\psi)$ can be determined by the following [*Wiesbeck et al.*, 2009]:

$$G(f,\theta,\psi) = \frac{4\pi f^2}{c_0^2}|H(f,\theta,\psi)|^2 \tag{9}$$

Fig. 2 shows the overall transmission line model for both the transmit and receive modes of the antenna. The use of two models is necessary because of the time derivative function of the transmit signal inherent to UWB antennas.

For the proposed transmission line model, the antenna transfer function, $H(\omega,\theta,\psi)$, will be modeled as a band pass filter. Some texts, such as [*Iam Opperman*, 2004] use the notation $A(\hat{k},\omega)$ and $h(\hat{k},\omega)$ to denote the transfer function (referred to as the *spatio-temporal transmit* and *spatio-temporal receive characteristic* respectively) where $\hat{k}$ is the incident field propagation direction instead of defining it in (θ,ψ) space as indicated above.

An ideal UWB antenna will have a smooth gain across the entire frequency band which will eliminate dispersion during transmission. However, this is not realizable. Because

of the Lorenz reciprocity constraint, $2j\omega h(-\hat{k},\omega) = c_0 A(\hat{k},\omega)$, which has a temporal derivative in the $j\omega$ term, the term $A(\omega) = 0$ when $\omega = 0$, and therefore hinders antenna radiation near $\omega = 0$ [*Di Benedetto et al.*, 2006]. Additionally, realization of a antenna with a relatively constant gain across the entire frequency spectrum is impossible, and as such all antennas are ultimately band limiting.

A typical UWB antenna has a >6:1 frequency range (i.e., the higher frequency is six times greater than the lower frequency) [*Taylor*, 1995]. This bandwidth results in significant issues pertaining to linearity and impedance matching across the operating frequency of the antenna [*Iam Opperman*, 2004]. For the purposes of the transmission line model and simulations, a perfect impedance match between the antenna and transmission line, prior to termination, is assumed. However, further anaylsis can be performed to refine the model to include impedance mismatches across the antenna operating frequency.

4.1. Re-radiation

The voltage induced in the received antenna by the incident electric field generates a current through both the antenna and load impedances of Fig. 2. Part of the signal power is transferred into the transmission line, and part of the power is absorbed and re-radiated by the antenna impedance. Secondly, part of the signal is reflected off of the termination impedance which is also re-radiated by the antenna. Both of these reverse traveling waves can constructively or destructively interfere with the forward propagating signal (V_0^+). Assuming that the antenna is perfectly matched to the transmission line (unlikely, but reasonable for modeling) than the magnitude of the first reverse traveling wave is minimized leaving only the reflection off of the termination, (V_0^-).

The power delivered by the antenna in receive mode at a location r_1 is (assuming matched polarizations) [*Di Benedetto et al.*, 2006]

$$P_{av} = \frac{|b^i|^2}{1-|\Gamma|^2} = \frac{4\pi||h(\hat{k},\omega)||^2}{1-|\Gamma|^2}\frac{||E^i(r_1,\hat{k},\omega||^2}{Z_0} \tag{10}$$

where b^i is the source strength impacting the antenna in receive mode defined as [*Di Benedetto et al.*, 2006]

$$b^i(\omega) = \sqrt{4/pi}h(\hat{k},\omega)\frac{E^i(r_1,\hat{k},\omega)}{\sqrt{Z_0}} \tag{11}$$

The process of illuminating the antenna with an incident plane wave results in an antenna-mode scattering process that consists of reception-reflection-reradiation [*Wang et al.*, 2010]. This can be modeled in the frequency domain using the antenna transfer functions previously identified. A significant complication though is that the reflection coefficient of the termination is not generally constant across the frequency range, as is typical of a narrow-band system [*T. Zwick*, 2013]. The calibration "short" and calibration "open" loads that have been experimentally examined generally have a constant reflection coefficient across the UWB frequency range. However, when dealing with other loads, the reflection coefficient will have a frequency dependence. The complete derivation of the resultant E-field at a distance, r, from the target antenna is derived as follows.

The channel transfer function can be modeled as Eq. 12 [*Wiesbeck et al.*, 2009] where r is the distance of the incident propagating interrogation wave from the target antenna as well as the distance the resultant re-radiated electromagnetic field is measured and used for the noise radar cross-correlation and c_o is the speed of light.

$$H_c = \frac{e^{j\omega r/c_0}}{2\pi r c_o} \tag{12}$$

Using Eq. 6, the voltage at the antenna terminals, U_{Rx}, due to the incident TEM wave propagating in the modeled channel, H_c, (V^+ in Fig. 2), is derived as:

$$U_{Rx}(\omega) = \mathbf{H}_{Rx}(\omega, \theta_{Rx}, \psi_{Rx}) \cdot \mathbf{H}_c(\omega) \cdot \sqrt{Z_{cRx}/Z_0} = V^+(\omega) \tag{13}$$

Because the distance the forward propagating TEM wave travels along the transmission line axis, z, is equivalent to the distance the reflected reverse propagating wave will travel, the reflected TEM wave can be derived simply as:

$$V^-(\omega) = V^+(\omega) \cdot \Gamma(\omega) \tag{14}$$

In which $\Gamma(w)$ is the frequency dependent reflection coefficient of the load, Z_L. The reflected TEM wave is the voltage incident on the antenna terminals for re-radiation, $U_{Tx} = U_{Rx} \cdot \Gamma(\omega)$. Thus, the re-radiated field strength, $E_{Tx}(\omega, r)$ at a distance r from is:

$$E_{Tx}(\omega, r) = \mathbf{H}_c(\omega) \cdot \mathbf{H}_{Tx}(\omega, \theta_{Tx}, \psi_{Tx}) j\omega U_{Tx}(\omega) \sqrt{Z_o/Z_{cTx}} \tag{15}$$

Assuming that the characteristic impedance of the antenna, Z_c is the same in both transmit and receive, as such $Z_{cRx} = Z_{cTx} = Z_c$. Also, the transfer function of the antenna is the reciprocal in both transmit and receive with the exception of a sign change indicative of reverse signal flow. Therefore, $\mathbf{H}_{Tx} = \mathbf{H}_{Rx} = \mathbf{H}_a$, and the overall equation relating the incident propagating TEM wave to the re-radiated electromagnetic field is:

$$E_{Tx}(\omega, r) = \mathbf{H}_c(\omega) \cdot \mathbf{H}_{Rx}(\omega, \theta_{Rx}, \psi_{Rx}) \cdot \mathbf{H}_{Tx}(\omega, \theta_{Tx}, \psi_{Tx}) \cdot \mathbf{H}_c(\omega) \cdot j\omega E_i(\omega, r, \theta, \psi) \cdot \Gamma(\omega) \tag{16}$$

$$= \Gamma(\omega) \cdot \mathbf{H}_c^2(\omega) \cdot |\mathbf{H}_a(\omega)|^2 \cdot j\omega E_i(\omega, r, \theta, \psi) \tag{17}$$

4.2. Full System Characterization

A plane wave propagating towards the bore sight of the antenna, while absolutely necessary for understanding the physics of the target-antenna model, is not practical for use

with the RF-DNA tools since a second antenna is necessary for reception of the transmitted signal reflected off the antenna load, Z_l. The two antennas therefore form a reciprocal link that can be fully characterized in the frequency domain using a similar transfer function approach. Assuming that both the transmit and receive (target) antennas are identical and operating in their respective far fields at a distance r, and that the bore sights of each antenna are facing each other, then the total analytical description of the transmitting propagation link in the frequency domain is as follows.

$$\frac{U_{Rx,1}(f)}{\sqrt{Z_{C,Rx}}} = \mathbf{H}_{Rx}^{T}(f,\theta_{Rx},\Psi_{Rx}) \cdot \frac{e^{j\ omegar/c}}{2\pi rc} \cdot \mathbf{H}_{Tx}(f,\theta_{Rx},\Psi_{Rx}) \cdot j\omega \frac{U_{Tx,1}(f)}{\sqrt{Z_{c,Tx}}}, \tag{18a}$$

$$U_{Tx,2}(f) = \Gamma(f) \cdot U_{Rx,1}(f), \tag{18b}$$

$$\frac{U_{Rx,2}(f)}{\sqrt{Z_{C,Rx}}} = \mathbf{H}_{Rx}^{T}(f,\theta_{Rx},\Psi_{Rx}) \cdot \frac{e^{j\ omegar/c}}{2\pi rc} \cdot \mathbf{H}_{Tx}(f,\theta_{Rx},\Psi_{Rx}) \cdot j\omega \frac{U_{Tx,1}(f)}{\sqrt{Z_{c,Tx2}}}. \tag{18c}$$

Note that 18b is derived from the reflection coefficient of a frequency dependent boundary, $V_r(f) = V_i(f)\Gamma(f)$ as indicated in [*Rao*, 1999]. Combining Eqs. 18, and assuming that the antennas are matched, results in the following full system derivation:

$$\frac{U_{Rx,1}(f)}{Z_{c,Rx}} = -\Gamma(f)\omega^2(\mathbf{H}^T \cdot \mathbf{H})_{Rx} \cdot (\mathbf{H}^T \cdot \mathbf{H})_{Tx} \cdot \frac{e^{2j\omega rc}}{(2\pi rc)^2} \cdot \frac{U_{Tx,1}}{Z_{cTx}} \tag{19}$$

Again, assuming $Z_{cRx} = Z_{cTx} = Z_c$ and $\mathbf{H}_{Tx} = \mathbf{H}_{Rx} = \mathbf{H}_a$, the model reduces to:

$$U_{Rx,1}(f) = -\Gamma(f)\omega^2(\mathbf{H}^T \cdot \mathbf{H})_a^2 \cdot \frac{e^{2j\omega rc}}{(2\pi rc)^2} \cdot U_{Tx,1}(f) \tag{20}$$

The time domain transmit and receive voltages, $u_{Tx}(t)$ and $u_{Rx}(t)$ can be determined using the Inverse Fast Fourier Transform (IFFT).

5. Simulations

The system response will be simulated using Matlab. In order to properly characterize the impact of bandwidth on the RF-DNA classification process, the full radar link

chain will be simulated. Therefore, transfer functions for the DNR transmit and receive antennas, H_{TxRx}, will be developed with an approximate bandwidth of 400-750 MHz as described in [*Ludwig*, 2012], with the assumption that matched antennas are used. Secondly, the target antenna will be characterized by a separate transfer function, H_T. Simulating the antenna as a filter will produce the desired frequency response, but will not simulate the dispersive nature of the antenna. Instead of characterizing the system in the frequency domain using multiple transfer functions, the system will be characterized in the time domain using Matlab's `filter` command and a series of cascaded digital filters. This allows for easier control the frequency response of the DNR transmit and receive antennas as well as the response of the target LPA antenna. A digital all-pass filter with an arbitrary group delay will be implemented to produce the desired time dispersion.

The input noise sequence is produced using Matlab's `randn` function which creates an array of simulated random White gaussian Noise (WGN). In order to restrict the bandwidth of the signal, a 10th order digital Butterworth filter using the same `butter` and `filter` commands will be used to create the equivalent filter model for the UWB antennas. Both the center frequency of the WGN noise signal and bandwidth can easily be adjusted to accommodate various illumination signals.

A final assumption made by this model, is to not include the effects of structural mode antenna scattering. It is not uncommon for an antenna structure to scatter more power than it absorbs [*Steyskal*, 2010]. However, that's assuming scatter in a sphere radiating from the antenna whereas the amount propagating directly back towards the interrogation signal source can actually be quite small. Scattering is also bandwidth dependent, since the power delivered to the load impedance is a function of the antenna input impedance

which can vary with frequency. However, the structural mode scatter is heavily dependent on antenna geometry and location relative to other objects (such as a ground plane). The time-domain response of the structural mode scatter requires a more thorough understanding of the target antenna and is heavily rooted in numerical solutions to Maxwell's equations, which would generally require the use of computer programs such as CST. While the structural mode scatter will add to the character of the antenna, its necessarily complicates the issue of how bandwidth will affect the RF-DNA fingerprints and associated classification algorithms.

5.1. Model Correlation Performance

The received signal from the full system model is correlated with Matlab's `xcorr` function. The results of the `xcorr` function applied to return signals off a modeled LPA with various noise interrogation signal bandiwidths is shown in Fig. 8. These results for the 100 MHz and 1 Ghz signal observationally correlate well with the correlation responses during previous experimentation [*Lukacs et al.*; *Zeqolari*, 2014].

5.2. Antenna Type Classification

For the first simulation, four antennas are iteratively interrogated. The center frequencies of the antenna-filter bandwidths are spaced at 450, 525, 600 and 675 MHz with a bandwidth of 750KHz each. The interrogation signal is centered at $f_c = 562MHz$, or approximately in between the 2nd and 3rd antenna relative frequency spacing, and the signal bandwidth is increased from 100KHz to 1GHz. Fig. 3 shows the results of this interrogation, as a percent of the MDA/ML classifier tool properly classifying the validation fingerprint against the "true" class that fingerprint belonged to. A new classification model

is constructed at each step increase in bandwidth. This approach was considered optimal because the user controls the interrogation waveform, and can choose the bandwidth that results in the optimal model performance. As is evident, none of the bandwidths achieved a classification above 50%. This is because of the relative location of the center frequency of the interrogation signal. As the interrogation signal bandwidth is widened, it excites the passband of the 2nd and 3rd antennas, but since they are identical antennas, they confuse with each other. As the bandwidth is increased, the 1st and 4th antennas are also excited, but again, they confuse with the response of the 2nd and 3rd antennas resulting in total confusion. Changing the center frequency of the interrogation signal to identically match the center frequency of a specific antenna significantly increased the classification performance of that antenna. This is shown in Fig. 4. In this simulation, the antennas remained the same, but the center frequency of the interrogation signal was increased to 600MHz. The 3rd antenna, with the bandwidth of 600-600.75MHz classified at above 90% across the span of interrogation bandwidths, whereas the other 3 antennas all remained at less than 40%. For this simulation, the bandwidth of the transmit antennas was set to approximately mirror the bandwidth of the DNR of 375-750MHz.

The second simulation extended the previous results, but with wideband antennas. Again, the antennas are spaced evenly with the previous center frequencies, but the bandwidth is increased to 150MHz for each antenna. The results are shown in Fig. 5. The 3rd antenna (centered at 600MHz - red in the chart) classified at over 90% across the interrogation signal iterative bandwidth, as expected based on the previous narrower band simulation. The 2nd and 4th antennas (450-600MHz and 600-750MHz bandwidth respectively) did not classify as well, and were often confused with each other as opposed to the

3rd antenna. The first antenna was surprising, achieving 100% across the board. Analysis of the resultant confusion matrices indicated that it did not confuse with any of the other three antennas. The filter model used to represent the antenna was a 4th order Butterworth filter implemented using Matlab's `butter` and `filter` commands. The simulated filter response only has about a 10dB magnitude difference between the peak of the pass-band and the center frequency of the interrogation signal (600MHz). `xcorr` is still able to derive a correlation result that is starkly different from the other three due to the center frequency spacing and bandwidth. Rerunning the simulation with an increased filter order (N=10), results in significantly improved classification for all 4 antennas, as shown in Fig. 6. Additionally, the classification performance is significantly less responsive to the interrogation signal bandwidth. Based on this, more important than the interrogation signal bandwidth is the frequency response of the target antennas.

5.3. Signal Attenuation Classification

In this simulation, the ability of the RF-DNA fingerprints with classifier algorithms to classify an attenuator placed between the antenna and the load is qualitative analyzed. To simulate the effect of the attenuator, the signal both before and after reflection from the load is attenuated by a scaling factor. Five different scale factors are used equivalent to the following values for the attenuator, $a_S = [0\ 3\ 6\ 9\ 12]$ dB. Initially, the DNR antennas and target antennas are assumed identical with a bandwidth of 375-750MHz. The noise signal has a center frequency, $f_c = 562$ MHz, in the middle of the antenna bandwidths. The bandwidth of the noise is varied from a bandwidth of approximately 90KHz to 900MHz. It is anticipated that the increased bandwidth will improve the performance of the classifier since the peak value of the sinc will scale larger with increased bandwidth, resulting in an

increased instantaneous amplitude response of the RF-DNA fingerprints in the correlation region. Also, since the noise signal is filtered to produce the desired bandwidth of the interrogation signal, the amount of energy contained within the instantaneous bandwidth is increasing as the bandwidth increases. Fig. 9 shows the percentage of time that the MDA/ML classifier correctly classified each attenuator value during model validation. Again, a new classification model is constructed for each step increase in interrogation signal bandwidth. The chart indicates that a narrow band signal has difficulty classifying all 5 attenuator values. As the bandwidth is increased, the ability to identify the first two attenuator values increased quickly, and the third increases as well, although not as fast. The 9dB and 12dB attenuation values do not increase significantly, probably because the correlation response is too small for those attenuator values and they confuse with each other across the interrogation signal bandwidth. These simulation results indicate interrogation signal bandwidth directly affects RF-DNA classification performance.

6. CONCLUSIONS

In conclusion, a literature review was conducted on the use of filters as antenna models, and the appropriate characteristics (such as the impulse repose, group delay and scatter) were evaluated. An analytical expression for the transfer function of the absorption and reflection of an electromagnetic wave incident on a passively terminated UWB antenna was derived. Finally, simulations were performed using Matlab that were chosen specifically to illustrate the performance of the RF-DNA fingerprints and classifiers using the antenna-filter model. Overall, the interrogation signal instantaneous bandwidth has a significant impact on classifier performance.

References

Di Benedetto, M., T. Kaiser, A. Molish, I. Oppermann, C. Politano, and D. Porcino (2006), *UWB Communication Systems: A Comprehensive Overview*, Hindawi Publishing Corporation.

Duda, R., P. Hart, and D. Stork (), *Pattern Classification*, John Wiley & Sons, Inc.

Hardin, J. A. (2013), Information Encoding on a Pseudo Random Noise Radar, Master's thesis, Air Force Inst of Tech, Dayton, OH.

Iam Opperman, J. L., Matti Hamalainen (2004), *UWB Theory and Applications*, John Wiley & Sons.

Klein, R., M. Temple, and M. Mendenhall (2009), Application of wavelet-based RF fingerprinting to enhance wireless network security, *Journal of Communications and Networks*, *11*(6), 544–554.

Ludwig, M. T. (2012), UHF Antenna Design for AFIT Random Noise Radar, Master's thesis, Air Force Inst of Tech, Dayton, OH.

Lukacs, M., P. Collins, M. Temple, and A. Zeqolari (), RF-DNA fingerprinting for antenna classification, *Accepted to Antennas and Wireless Propogation Letters*.

Lynchi, D. (2004), *Introduction to RF Stealth*, Scitech Publishing, Inc.

Mohammadian, A., A. Rajkotia, and S. Soliman (2003), Characterization of uwb transmit-receive antenna system, in *Ultra Wideband Systems and Technologies, 2003 IEEE Conference on*, pp. 157–161, doi:10.1109/UWBST.2003.1267823.

Papio-Toda, A., W. Sorgel, J. Joubert, and W. Wiesbeck (2007), Uwb antenna transfer property characterization by fdtd simulations, in *Antennas, 2007. INICA '07. 2nd International ITG Conference on*, pp. 81–85, doi:10.1109/INICA.2007.4353937.

Priestly, J. A. (2011), AFIT NoNet: Software Model Development and Optimization of Signal Processing Architecture, Master's thesis, Air Force Inst of Tech, Dayton, OH.

Rao, S. M. (1999), *Time Domain Electromagnetics*, Elsevier, San Diego, CA.

Reising, D. R. (2012), Exploitation of RF-DNA for Device Classification and Verification Using GRLVQI Processing, Master's thesis, Air Force Inst of Tech, Dayton, OH.

Schmitt, A. L. (2009), Radar Imaging with a Network of Digital Noise Radar Systems, Master's thesis, Air Force Inst of Tech, Dayton, OH.

Steyskal, H. (2010), On the power absorbed and scattered by an antenna, *Antennas and Propagation Magazine, IEEE*, *52*(6), 41–45, doi:10.1109/MAP.2010.5723219.

T. Zwick, J. T., W. Wiesbeck (2013), *Ultra-wideband RF Systems Engineering*, Cambridge University Press, New York, NY.

Taylor, J. (1995), *Introduction to Ultra-Wideband Radar Systems*, CRC Press, Inc.

Wang, W.-T., Y. Liu, S.-X. Gong, Y.-J. Zhang, and X. Wang (2010), Calculation of Antenna Mode Scattering Based on Method of Moments, *Progress in Electromagnetics Research Letters*, *15*, 117–126.

Wiesbeck, W., G. Adamiuk, and C. Sturm (2009), Basic properties and design principles of uwb antennas, *Proceedings of the IEEE*, *97*(2), 372–385.

Wilson, R., and P. Collins (2013), Noise radar as an indoor navigation aide, in *Proceedings of the Antenna Measurement Techniques Association 35th Symposium*, Columbus, OH.

Zeqolari, A. (2014), Ultra-Wideband Radio Frequency Fingerprinting, Master's thesis, Air Force Inst of Tech, Dayton, OH.

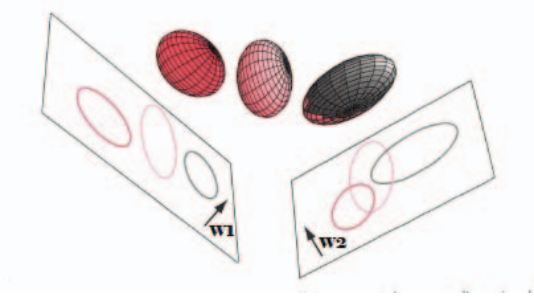

Figure 1. MDA/ML classification of fingerprint in a 3-class problem [*Duda et al.*]

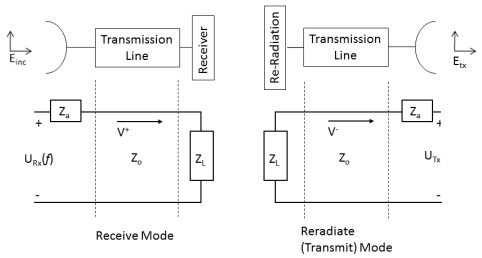

Figure 2. Proposed transmission line model for target antenna under test

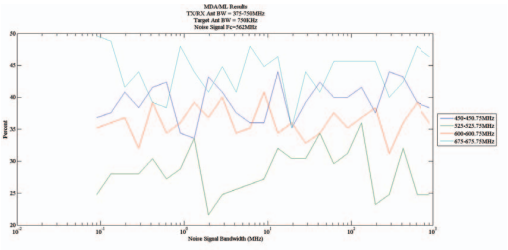

Figure 3. MDA/ML classifier performance for 4 broadband antennas with an interrogation signal center frequency of 562MHz

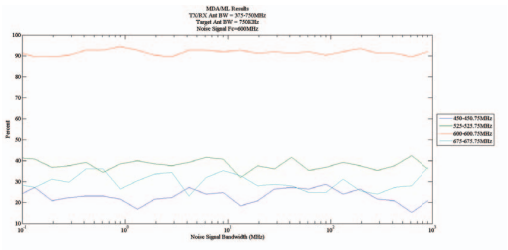

Figure 4. MDA/ML classifier performance for 4 broadband antennas with an interrogation signal center frequency of 600MHz

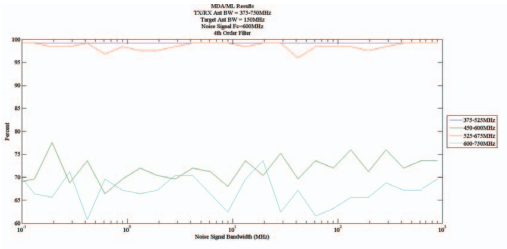

Figure 5. MDA/ML classifier performance for 4 wideband antennas with an interrogation signal center frequency of 600MHz (4th order filter approximation)

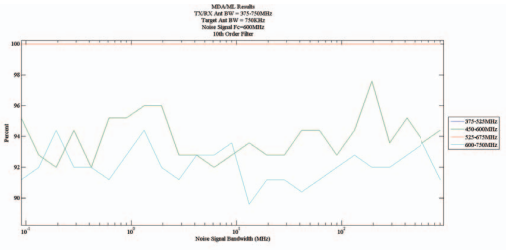

Figure 6. MDA/ML classifier performance for 4 wideband antennas with an interrogation signal center frequency of 600MHz (10th order filter approximation)

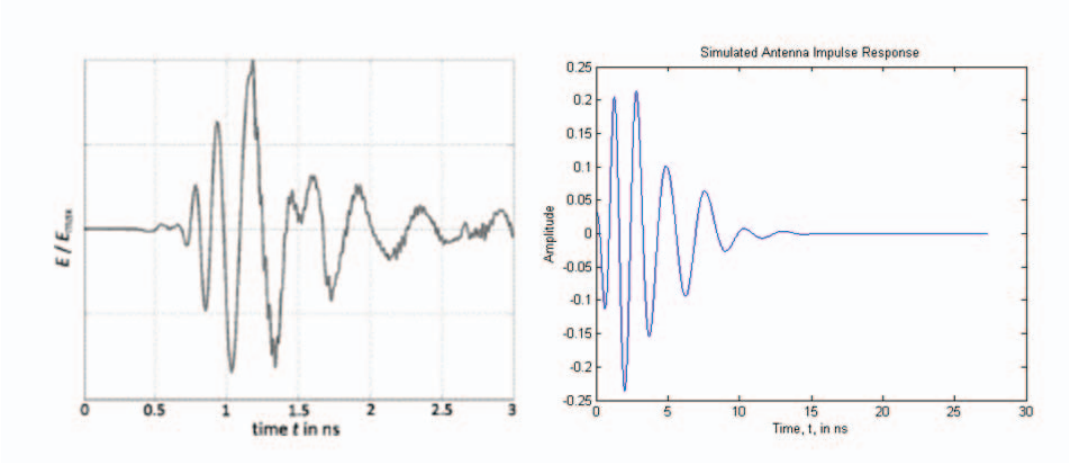

Figure 7. Measured versus Simulated Impulse Response of the Transmit and Receive DNR LPA antennas with simulated Group Delay

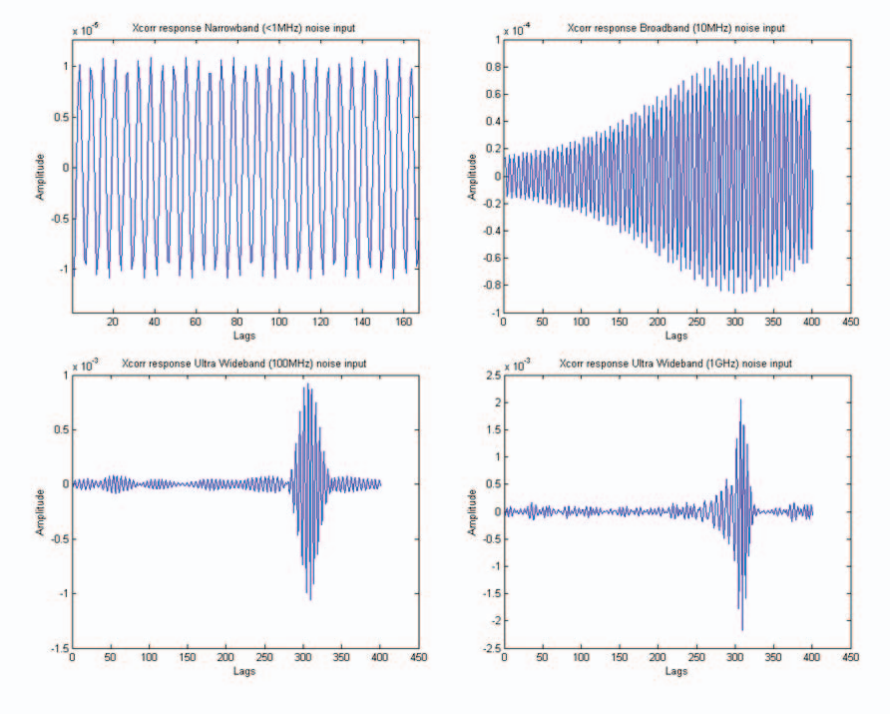

Figure 8. Simulated XCORR System response to a <1MHz (top left), 10MHz (top right), 100MHz (bottom left) and 1GHz (bottom right) bandwidth interrogation signal

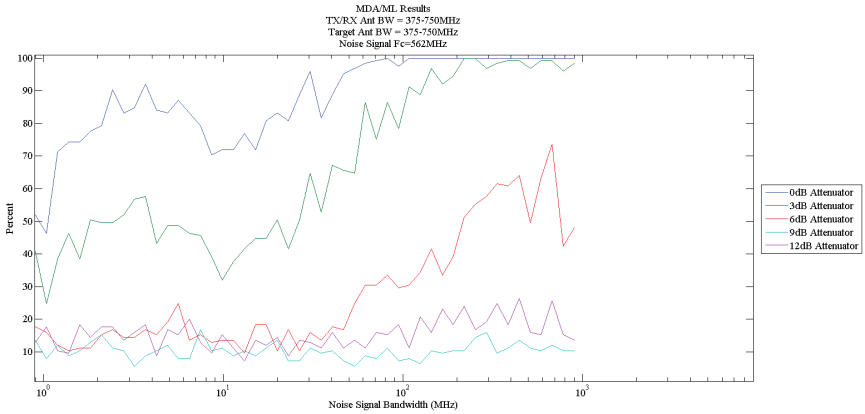

Figure 9. MDA/ML classifier performance for identifying attenuation values